

## Article

# Insight into the FCC→HCP Transformation in Co-Rich Co-Cr-Fe-Mn-Ni High-Entropy Alloys

Yuchen Wang<sup>1</sup>, Changjun Wu<sup>1,2,\*</sup> , Ya Liu<sup>1,2</sup> , Mengyun Tian<sup>1</sup>, Xiaowang Lu<sup>3</sup> and Xuping Su<sup>1,2</sup> 

- <sup>1</sup> Jiangsu Key Laboratory of Materials Surface Science and Technology, School of Materials Science and Engineering, Changzhou University, Changzhou 213164, China
- <sup>2</sup> Jiangsu Collaborative Innovation Center of Photovoltaic Science and Engineering, Changzhou University, Changzhou 213164, China
- <sup>3</sup> School of Materials Science and Engineering, Yancheng Institute of Technology, Yancheng 224051, China
- \* Correspondence: wucj@cczu.edu.cn

**Abstract:** The existence of an HCP phase in FCC-type high-entropy alloys can improve the alloy's mechanical properties. In many cases, an HCP phase is induced by deformation. In the present work, an FCC to HCP transition was detected during the cooling of Co<sub>1.5</sub>CrFeMnNi<sub>0.5</sub> and Co<sub>1.75</sub>CrFeMnNi<sub>0.25</sub> alloys. Therefore, arc-melted annealed Co<sub>x</sub>CrFeMnNi<sub>2-x</sub> (x = 0.25–1.75) alloys that were then subjected to long-term vacuuming were investigated using XRD, DSC, HT-XRD, thermodynamic calculation, and first-principle calculation. It was confirmed that the FCC to HCP transition occurred at ~450 °C during the cooling of the alloys with x ≥ 1.5. The volume fraction of the HCP phase increased with Co content. It was proven that the HCP phase was not stable above 600 °C. First-principle calculations further indicated that the HCP structure was more stable than the FCC structure for Co<sub>1.75</sub>CrFeMnNi<sub>0.25</sub> alloy, and there was a likelihood of an FCC to HCP transition. Moreover, experimental tests confirmed that the microhardness of the Co<sub>1.75</sub>CrFeMnNi<sub>0.25</sub> alloy reached 213 HV because it contained a substantial HCP phase. This value is much higher than those of other non-HCP-containing alloys, either in their as-cast states or after annealing. These results provide guidance for the design of FCC-type high-entropy alloys with desirable mechanical properties through HCP phase strengthening.



**Citation:** Wang, Y.; Wu, C.; Liu, Y.; Tian, M.; Lu, X.; Su, X. Insight into the FCC→HCP Transformation in Co-Rich Co-Cr-Fe-Mn-Ni High-Entropy Alloys. *Metals* **2023**, *13*, 504. <https://doi.org/10.3390/met13030504>

Academic Editor: Normen Fuchs

Received: 20 January 2023  
Revised: 15 February 2023  
Accepted: 27 February 2023  
Published: 2 March 2023



**Copyright:** © 2023 by the authors. Licensee MDPI, Basel, Switzerland. This article is an open access article distributed under the terms and conditions of the Creative Commons Attribution (CC BY) license (<https://creativecommons.org/licenses/by/4.0/>).

**Keywords:** high-entropy alloys; HCP phase; phase stability; phase transition; alloy strengthening

## 1. Introduction

As emerging structural materials, high-entropy alloys (HEAs) have rapidly garnered much attention for transforming the conventional alloy design concept by shifting the search space of useful alloys from the corners of phase diagrams to their central regions [1,2]. HEAs always exhibit superior properties over traditional alloys, such as high strength, high hardness, high-temperature resistance, wear resistance, oxidation resistance, and corrosion resistance [3–6]. Co-Cr-Fe-Mn-Ni high-entropy alloys have become the most intensively studied systems due to their excellent FCC phase stability, good strength and ductility, and excellent fracture resistance at low temperatures [3,7,8]. Because the atomic radius and electronegativity of each element in the alloy system are very close to each other and the diffusion rate of each atom is relatively slow, the system has good chemical compatibility [9–12]. Cantor et al. [13] found that CoCrFeMnNi high-entropy alloys, in fact, have a single FCC phase. Subsequently, they published a related paper in *Science* [14], which proposed, for the first time, that the fracture toughness of Co-Cr-Fe-Mn-Ni high-entropy alloys is unexpectedly high, at 77–293 K. The tensile strength and yield strength reach 450 MPa and 125 MPa, respectively, while the elongation reaches 80%. At 77 K, the tensile strength and yield strength of a Co-Cr-Fe-Mn-Ni high-entropy alloy reach 1280 MPa and 759 MPa, respectively, and its elongation is slightly higher than that at room temperature [14]. The reason for this is that there are many twin boundaries and dislocations in Co-Cr-Fe-Mn-Ni high-entropy alloys

at low temperatures, which enhance the properties of the alloy. The excellent properties of Co-Cr-Fe-Mn-Ni high-entropy alloys are often considered to be related to the lattice distortion and diffusion obstruction caused by mixing with various principal elements. The plastic deformation of high-entropy alloys is usually caused by dislocation slips at room temperature and at low temperatures. Due to the decrease in stacking fault energy (SFE), the plastic deformation mode changes from dislocation slip to deformation twins [15], which improves the mechanical properties of high-entropy alloys.

Many low-SFE metals and alloys have excellent tensile properties and high levels of elongation at room temperature due to the TWIP (twinning-induced plasticity) and TRIP (transformation-induced plasticity) effects; examples include TWIP steel, metastable austenitic steel, and TRIP steel. Therefore, a material's chemical composition can be appropriately changed to reduce the SFE, thus promoting the generation of Shockley dislocation and the occurrence of twin- and strain-induced FCC→HCP martensitic transformations [16]. In addition, Co-rich high-entropy alloys usually exhibit FCC and HCP crystal structures. The FCC phase is usually stable at high temperatures, while the HCP phase tends to be stable at decreasing temperatures. The SFE values of these alloys are generally very low and even negative at room temperature for some component alloys [17]. This promotes the FCC→HCP martensitic transformation and improves the mechanical properties of the alloy. Phase composition seriously affects the properties of alloys. The FCC phase is soft and plastic, while the HCP phase is hard and not plastic. Therefore, when an alloy undergoes strain-induced FCC→HCP martensitic transformation, the martensite HCP phase plays a "secondary hardening" effect, which greatly improves the overall hardness of the alloy.

Wei et al. [18] conducted an in-depth study on a Co-rich CoCrFeNi high-entropy alloy and found that it was the lattice distortion and slow diffusion effect caused by the mixing of various principal elements that produced the superior mechanical properties of the alloys. The only plastic deformation mode of the alloy at room temperature is dislocation slip, but deformation twins occur at low temperatures due to the decrease in SFE. The SFE of the CoCrFeNi alloy is calculated to be about 20–30 mJ/m<sup>2</sup> at room temperature, which is approximately zero at 0 K, indicating that the HCP phase gradually tends towards stability with the decrease in temperature. In addition, Mn, Ni, and Fe are the FCC phase stabilizers, while Co and Cr are the HCP phase stabilizers of the Co-based alloys [19]. The results showed that, in the CoCrFeNi alloy, increasing the Co content at the expense of decreasing the Fe and Ni content can effectively reduce the SFE value and the FCC phase stability; the deformation mechanism also changes from the original deformation twin to an FCC→HCP martensitic transformation. Co<sub>35</sub>Cr<sub>25</sub>Fe<sub>20</sub>Ni<sub>20</sub> and Co<sub>45</sub>Cr<sub>25</sub>Fe<sub>15</sub>Ni<sub>15</sub> alloys with metastable single FCC phases have better strength and tensile properties than other single FCC phase alloys because they can promote the formation of twins and FCC→HCP transformation [20].

In addition, Wei et al. [16] noted that Co-based alloys have better mechanical properties than other alloys. The SFE of the Ni<sub>15</sub>Fe<sub>15</sub> alloy is slightly lower than that of CoCrFeMnNi, which makes deformation twins more likely to occur. Due to the TWIP effect, both strength and ductility are greatly improved. In addition, the further decrease in SFE in Ni<sub>15</sub>Fe<sub>10</sub> leads to the transformation of the deformation mode from deformation twin to FCC→HCP transition; this significantly increases the strength due to the TRIP effect. Due to the TWIP and TRIP effects induced by the FCC→HCP transition, the tensile strength of Co<sub>35</sub>Cr<sub>20</sub>Mn<sub>15</sub>Ni<sub>15</sub>Fe<sub>15</sub> and Co<sub>35</sub>Cr<sub>25</sub>Mn<sub>15</sub>Ni<sub>15</sub>Fe<sub>10</sub> alloys reaches 688 MPa and 806 MPa, respectively, and the elongation reaches 96% and 76%, respectively. These results are superior to those found for equal-atomic-ratio and Fe-rich non-equal-atomic-ratio alloys. Chung et al. [21] also carried out an in-depth study on the deformation mechanisms in the plastic deformation process of high-entropy alloys; the results showed that the deformation mechanism of the Cr-Ni-Mn-Fe alloy at room temperature was deformation twinning, but, at low temperatures, it was transformed into the combined effect of TWIP and TRIP, which greatly improved the tensile properties of the alloy [21]. In short, both deformation twinning and FCC→HCP martensitic transformation are instrumental in obtaining

high-performance and high-entropy alloys. The SFE of each component element affects the SFE of the whole alloy. When the concentrations of Co and Cr increase and the concentrations of Mn and Fe decrease, the phase stability of FCC and SFE can be reduced and the comprehensive mechanical properties of the alloy can be improved [22,23]. Therefore, the  $\text{Co}_{35}\text{Cr}_{25}\text{Mn}_{15}\text{Ni}_{15}\text{Fe}_{10}$  alloy undergoes an FCC to HCP transformation in the process of plastic deformation, and its tensile properties are greatly improved. This provides a feasible basis for further study of the development of high-performance, high-entropy alloys. Moreover, the HCP phase was also found in  $\text{Co}_{35}\text{Cr}_{25}\text{Fe}_{40-x}\text{Ni}_x$  ( $x = 0\text{--}15$ ) alloys after tensile testing [24].

In a previous work conducted by our group, Wang et al. [25] found that a small amount of HCP phase existed in the 600~1000 °C annealed  $\text{Co}_{1.5}\text{CrFeMnNi}_{0.5}$  alloy. Meanwhile, no HCP phase was found in  $\text{Co}_{1.25}\text{CrFeMnNi}_{0.75}$  [25] or  $\text{Co}_{1.5}\text{CrFeMn}_{0.5}\text{Ni}$  [26]. As discussed above, the HCP phase forms after deformation or under high temperatures [16,27,28]. To accurately understand the stability of the HCP phase and the FCC to HCP phase transition,  $\text{Co}_x\text{CrFeMnNi}_{2-x}$  ( $x = 0.25\text{--}1.75$ ) alloys were investigated in the present work.

## 2. Materials and Methods

A series of  $\text{Co}_x\text{CrFeMnNi}_{2-x}$  ( $x = 0.25, 0.5, 0.75, 1.25, 1.5, 1.75$ ) high-entropy alloys were designed. To clearly show their composition, the alloys are briefly referred to as  $\text{Co}_5\text{Ni}_{35}$ ,  $\text{Co}_{10}\text{Ni}_{30}$ ,  $\text{Co}_{15}\text{Ni}_{25}$ ,  $\text{Co}_{25}\text{Ni}_{15}$ ,  $\text{Co}_{30}\text{Ni}_{10}$ , and  $\text{Co}_{35}\text{Ni}_5$ . All the raw materials (Co, Cr, Fe, Mn, and Ni granules) have a purity higher than 99.95 wt.%. The alloy was melted in a non-consumable magnetically controlled arc-melt furnace under the protection of high-purity argon gas after oxygen absorption by Ti. The total mass of each sample was 10 g. In order to ensure uniform melting composition, each ingot was melted at least four times. Subsequently, each ingot was cut into four pieces by wire cutting; one of them was used for as-cast analysis, and the others were sealed individually in evacuated quartz tubes and then annealed at 1000 °C, 800 °C, or 600 °C for 720 h. At the end of the treatment, the alloys were quenched in cold water. The phase constituents of the alloys in the as-cast state and after annealing were studied.

X-ray diffraction (XRD) analysis using a D/max 2500 PC X-ray diffractometer with Cu K $\alpha$  radiation was used to identify the phases in the alloys. In addition, a PANalytical EMPYREAN variable-temperature X-ray diffraction analyzer was used to test and analyze some of the alloys. The microstructure and composition of the alloys were observed using a JSM-6510 scanning electron microscope (SEM) equipped with an Oxford Energy Spectrometer (EDS). Differential scanning calorimetry (DSC) tests were carried out to obtain the phase transition points of the high-entropy alloys. A NETZSCH DSC404 differential scanning calorimeter was used in the experiment, and the heating rate was set at 20 K/min or 5 K/min. An HXD-1000TMC/LC Vickers hardness tester was used to test and analyze microhardness.

To understand the tendencies of the FCC to HCP transformation, a first-principle calculation for the HCP-containing alloys was carried out based on the plane-wave pseudopotential method. Virtual lattice approximation (VCA) [29–31] was used to build the crystal cells so as to reasonably predict the phase stability of the alloy system [32]. In addition, the PBE function under generalized gradient approximation (GGA) was used to calculate the correlation function of the electron exchange, and the interaction between the electrons and ions was processed using OTFG ultrasoft pseudopotentials (USPP). The truncation energy of the plane-wave function expansion was calculated as 630 eV, the spacing between the grids of K points in the inverted space was 0.4 nm<sup>-1</sup>, and the grids were divided into 9 × 9 × 9 (FCC) or 12 × 12 × 6 (HCP) units [33,34]. To obtain the minimum energy level, the structure of the cell is fully optimized. The total energy tolerance is 10<sup>-5</sup> eV/atom, the force tolerance is 0.03 eV/Å, the maximum stress is 0.05 GPa, and the maximum displacement is 0.001 Å [35].

### 3. Results

#### 3.1. Phase Constituents of the As-Cast $\text{Co}_x\text{CrFeMnNi}_{2-x}$ Alloys

The phase constituents of the as-cast  $\text{Co}_x\text{CrFeMnNi}_{2-x}$  alloys were first examined using XRD. It was confirmed that the as-cast  $\text{Co}_5\text{Ni}_{35}$ – $\text{Co}_{25}\text{Ni}_{15}$  alloys were composed of a single FCC solid solution, which is consistent with the results presented in our previous work [25]. For brevity, the XRD patterns and detected chemical composition of the alloys  $\text{Co}_5\text{Ni}_{35}$ – $\text{Co}_{15}\text{Ni}_{25}$ , with a single FCC phase, are not shown here again. The XRD patterns of the alloys  $\text{Co}_{25}\text{Ni}_{15}$ – $\text{Co}_{35}\text{Ni}_5$  are presented in Figure 1. It is clear that the as-cast alloys  $\text{Co}_{30}\text{Ni}_{10}$  and  $\text{Co}_{35}\text{Ni}_5$  are composed of the FCC + HCP phases. The strong HCP characteristic peaks indicate the high volume fraction of the HCP phase in the  $\text{Co}_{35}\text{Ni}_5$  alloy. However, no contrast or composition differences between FCC and HCP were found in the SEM-EDS analysis, a result that is consistent with [15]. It was confirmed that uniform alloys were obtained, and the actual composition of the alloys was almost the same as that of the designed alloy. Therefore, it can be deduced that the HCP phase has a composition similar to or the same as that of the FCC phase.

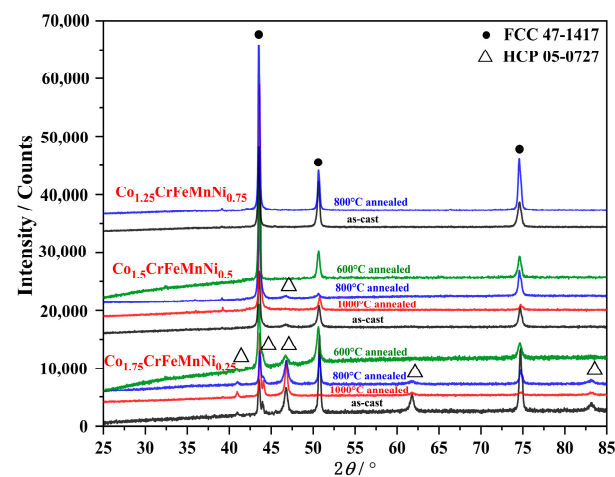


**Figure 1.** The XRD patterns of the as-cast or annealed  $\text{Co}_x\text{CrFeMnNi}_{2-x}$  alloys.

As found in [25], a small amount of HCP phase was found in a  $\text{Co}_{1.5}\text{CrFeMnNi}_{0.5}$  alloy annealed at 600–1000 °C. It is well-known that prolonged annealing is a good method for investigating phase stabilities [36,37]. To determine the phase stability of the HCP phase, the as-cast alloys were annealed at 600, 800, or 1000 °C for 720 h. The XRD patterns shown in Figure 1 indicate that the HCP phase still exists in the annealed alloys  $\text{Co}_{30}\text{Ni}_{10}$  and  $\text{Co}_{35}\text{Ni}_5$ . That is to say, the annealing temperature and annealing time had almost no effect on the stability of the HCP phase in the  $\text{Co}_x\text{CrFeMnNi}_{2-x}$  alloys. Moreover, as shown in Figure 2, a small amount of Cr-rich black BCC phase was found in the phase boundary of the  $\text{Co}_{25}\text{Ni}_{15}$  and  $\text{Co}_{30}\text{Ni}_{10}$  alloys annealed at 800 °C. Their chemical compositions, which were detected by SEM-EDS, are presented in Table 1. The composition of the BCC phase in 800 °C annealed  $\text{Co}_{25}\text{Ni}_{15}$  alloy is detected to be 6.9Co-68.9Cr-7.0Fe-12.4Mn-4.7Ni (at.%). This is similar to the Cr-rich BCC phase in the  $\text{CoCrFeMn}_{0.75}\text{Ni}_{1.25}$  alloy annealed at 800 °C described in [25]. As can be seen in Table 1, the BCC phase in 800 °C annealed  $\text{Co}_{30}\text{Ni}_{10}$  alloy contains much lower Cr content and much higher Co content. This is because the phase size is smaller than that in the 800 °C annealed  $\text{Co}_{25}\text{Ni}_{15}$  alloy, as shown in Figure 2b. The detected composition may relate to BCC + FCC two phases. Because the volume fraction of the Cr-rich BCC phase is too limited to be detected by XRD, there are no BCC peaks in XRD patterns. The appearance of the BCC phase, as shown in Figure 2a,b, indicated that it precipitated in the FCC phase boundary. In Reference [25], when the  $\text{Co}_x\text{CrFeMnNi}_{2-x}$  alloys were annealed at 800 °C for 360 h, there was no Cr-rich BCC precipitate. That is to say, prolonging the annealing time at 800 °C will promote the precipitation of the BCC phase in the FCC phase boundary.

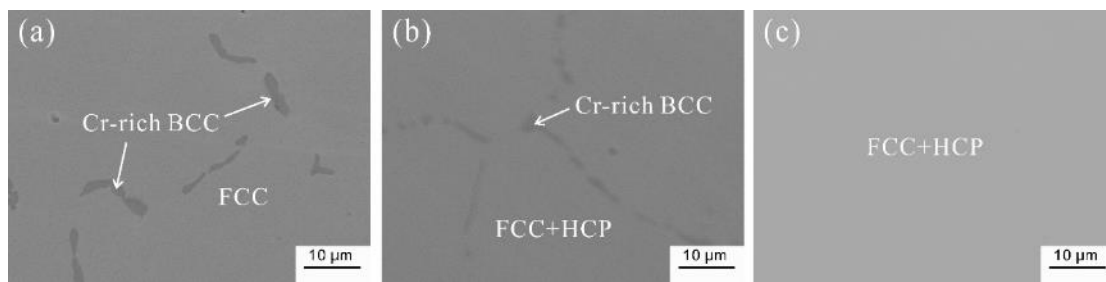


**Figure 2.** SEM images of the  $\text{Co}_x\text{CrFeMnNi}_{2-x}$  alloys annealed at 800 °C. (a)  $\text{Co}_{25}\text{Ni}_{15}$ ; (b)  $\text{Co}_{30}\text{Ni}_{10}$ ; (c)  $\text{Co}_{35}\text{Ni}_5$ .

**Table 1.** The detected chemical composition of phases in the  $\text{CoCrFeMn}_x\text{Ni}_{2-x}$  alloys at the as-cast or annealed states.

Alloys	States	Phases	Detected Composition (at.%)				
			Co	Cr	Fe	Mn	Ni
$\text{Co}_{25}\text{Ni}_{15}$	as-cast	FCC	25.2	19.8	20.0	20.7	14.3
	1000 °C annealed	FCC	23.8	19.8	19.2	20.9	16.3
	800 °C annealed	FCC	25.7	19.7	20.4	20.7	13.5
		BCC	6.9	68.9	7.0	12.4	4.7
$\text{Co}_{30}\text{Ni}_{10}$	as-cast	FCC/HCP	31.1	20.9	22.3	16.5	9.2
	1000 °C annealed	FCC	31.1	21.6	21.0	16.4	9.9
	800 °C annealed	FCC	31.2	20.6	19.7	19.3	9.2
		BCC	17.7	47.5	13.5	15.5	5.9
$\text{Co}_{35}\text{Ni}_5$	as-cast	FCC/HCP	35.1	19.9	19.9	20.2	4.9
	1000 °C annealed	FCC/HCP	37.0	19.3	19.6	18.9	5.2
	800 °C annealed	FCC/HCP	35.1	19.7	19.9	20.2	5.1

### 3.2. DSC Examination

In order to identify the phase transformation point in the  $\text{Co}_x\text{CrFeMnNi}_{2-x}$  alloys, all the as-cast alloys were examined using DSC at a rate of 20 K/min. The DSC heating curves are presented in Figure 3. There is an obvious endothermic peak at 1250–1300 °C, which should correspond to the solidus temperature. As can be seen from Figure 3, the solidus temperature of the  $\text{Co}_x\text{CrFeMnNi}_{2-x}$  alloys increased with Co content, from 1252 °C ( $\text{Co}_5\text{Ni}_{35}$ ) to 1292 °C ( $\text{Co}_{25}\text{Ni}_{15}$ ). The asymmetric shape of the endothermic peak means that there is a small temperature difference between the liquidus and the solidus. Below 1200 °C, there is no obvious DSC peak, i.e., there is no reaction with a severe thermal effect below 1200 °C. As for the DSC curve of the  $\text{Co}_{35}\text{Ni}_5$  alloy, as shown in Figure 3b, the baseline changed slightly at 450 °C, which indicates that a phase transformation may exist and may relate to the HCP→FCC transition.

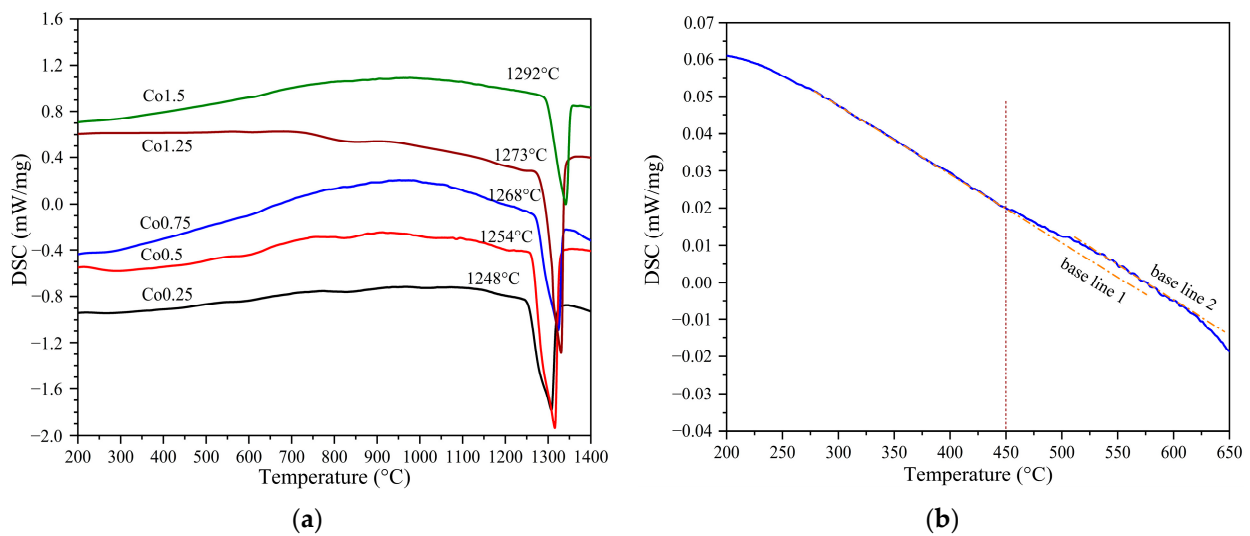


**Figure 3.** The DSC heating curves of the as-cast  $\text{Co}_x\text{CrFeMnNi}_{2-x}$  alloy. (a)  $\text{Co}_5\text{Ni}_{35}\text{-Co}_{30}\text{Ni}_{10}$ ; 20 K/min; (b)  $\text{Co}_{35}\text{Ni}_5$ , 5 K/min.

### 3.3. High-Temperature XRD Examination

To elucidate the HCP  $\rightarrow$  FCC transformation, the as-cast  $\text{Co}_{35}\text{Ni}_5$  alloy was examined using XRD at variable temperatures. According to the DSC results shown in Figure 3b, a transformation may occur close to 450 °C. Therefore, the high-temperature XRD test was performed at 420 °C, 600 °C, and 800 °C. As shown in Figure 4, the intensity of the HCP peaks dramatically weakened at 420 °C, and there was no HCP peak at 600 °C. This result confirms that there is an HCP  $\rightarrow$  FCC transformation during the heating of the as-cast  $\text{Co}_{35}\text{Ni}_5$  alloy. The transformation starts near 420 °C, which concurs with the DSC results (Figure 3b). When the XRD test was performed at 800 °C, large amounts of MnO were detected, as shown in Figure 4. Although the high-temperature XRD experiment was carried out in an argon-heavy atmosphere, manganese oxide can still form. Nonetheless, no HCP phase exists at 800 °C.

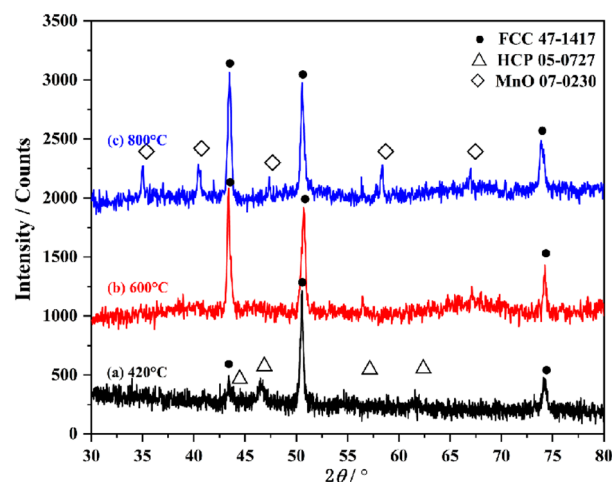


**Figure 4.** XRD patterns of  $\text{Co}_{1.75}\text{CrFeMnNi}_{0.25}$  at varying temperatures.

### 3.4. Phase Diagram

To understand the phase stability and phase transformation of the investigated alloys, the vertical section of the  $\text{Co}_x\text{CrFeMnNi}_{2-x}$  system was thermodynamically calculated in the present work. Various thermodynamic databases were used, including PanHEA, PanFe, PanCo, PanNi, and TCFE. However, the HCP phase was not stable in all the calculated vertical sections. A phase diagram, which was calculated based on the TCFE database, has

better agreement with the experimental results and is shown in Figure 5. As presented above, in the present work, the as-cast  $\text{Co}_x\text{CrFeMnNi}_{2-x}$  alloys were annealed at 600, 800, or 1000 °C for 720 h. The detected phase constituents in the quenched alloys and the DSC results are also shown in Figure 5. Because of the existence of an FCC→HCP transformation during cooling, an HCP phase is detected in the quenched  $\text{Co}_{35}\text{Ni}_5$  alloy.

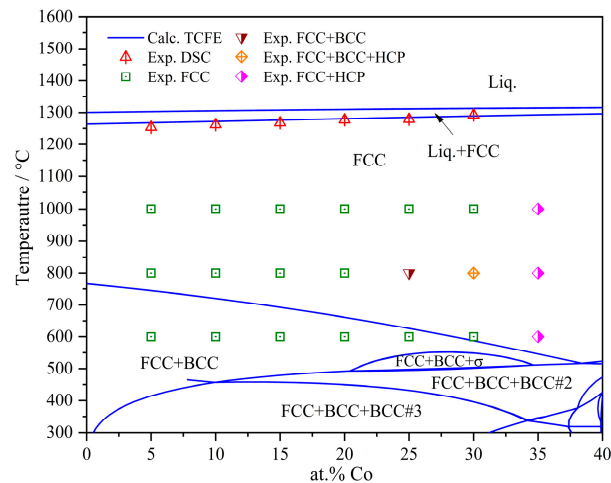


**Figure 5.** A vertical section of the  $\text{Co}_x\text{CrFeMnNi}_{2-x}$  system calculated using the TCFE database. The phase constituents in the annealed and quenched alloys and the DSC results are shown in the figure.

As can be seen from Figure 5, the calculated solidus temperature is consistent with the DSC results. There is a narrow temperature range between the solidus and the liquidus. Therefore, the endothermic peak in the DSC curve (Figure 3) has an asymmetric shape. It is clear that just a single FCC phase region exists below the solidus. For this reason, a uniform FCC phase can be obtained in as-cast alloys. In addition, the calculation predicted an FCC + BCC phase region below the FCC region, which conflicts with the experimental result of a single FCC phase [38].

In the Co-Cr-Fe-Mn-Ni alloys, Mn, Ni, and Fe are the FCC phase stabilizers. If the concentration of Mn, Ni, or Fe increases, it can stabilize the FCC phase and increase SFE; Co and Cr are HCP phase stabilizers. If the concentration of Co or Cr increases, it can stabilize the HCP phase and decrease SFE.

It is well known that, for pure Co, an FCC→HCP polymorphic transformation occurs at 422 °C during cooling. According to the DSC test and the high-temperature XRD test, the FCC→HCP transformation of the  $\text{Co}_{35}\text{Ni}_5$  alloy occurs around 420 °C, which is close to the transformation temperature of pure Co. Moreover, according to the related sub-binary systems, there is an FCC→HCP transformation on the Co-rich side. Generally, the HCP is stable when Co content is above 60%. The dissolution of Mn, Fe, and Ni in FCC-Co decreases the polymorphic transformation temperature, while the presence of Cr can increase the transformation temperature. In the present work, the HCP phase was found in the quenched  $\text{Co}_{35}\text{Ni}_5$  alloy, i.e., the FCC→HCP transformation is fast and constitutes a diffusionless transformation. Therefore, there is no contrast or composition difference between the FCC and HCP phases.

As mentioned above, the FCC phase is stable at high temperatures, while the HCP phase is stable at room temperature. This is consistent with the FCC→HCP martensitic transformation process of the  $\text{Co}_{35}$  alloy during plastic deformation, which was identified by Wei et al. [16,18], although the formation mechanism is slightly different. The formation of the HCP phase in the  $\text{Co}_{35}$  alloy arises due to the composition change; that is, the increase in the Co and Cr concentrations or the decrease in the Mn and Fe concentrations can reduce the phase stability of FCC and SFE. Thus, the FCC→HCP martensitic transformation occurs during the plastic deformation of the alloy. In the present work, although the  $\text{Co}_{35}\text{Ni}_5$  alloy did not undergo plastic deformation, the FCC→HCP phase transformation still occurred

during cooling. Since every element in a high-entropy alloy system occupies a randomly disordered lattice, Cr, Fe, Mn, and Ni will randomly occupy the lattice of Co. Therefore, the FCC→HCP transition point of the  $\text{Co}_{35}\text{Ni}_{15}$  alloy is slightly higher than that of pure Co.

### 3.5. Alloy Hardness

To analyze the effect of the FCC→HCP transformation on the mechanical properties of the alloys, the microhardness of the as-cast and annealed  $\text{Co}_x\text{CrFeMnNi}_{2-x}$  alloys were examined. As shown in Figure 6, the microhardness of  $\text{Co}_{35}\text{Ni}_{15}$  is much higher than that of the other as-cast or annealed alloys. This phenomenon can be attributed to the FCC→HCP transformation during cooling in the  $\text{Co}_{35}\text{Ni}_{15}$  alloy. The plasticity of the HCP phase is poorer than that of the FCC phase; the HCP phase acts as a hardening phase, meaning that the dispersed HCP structure strengthens the FCC matrix, greatly improving strength and hardness.

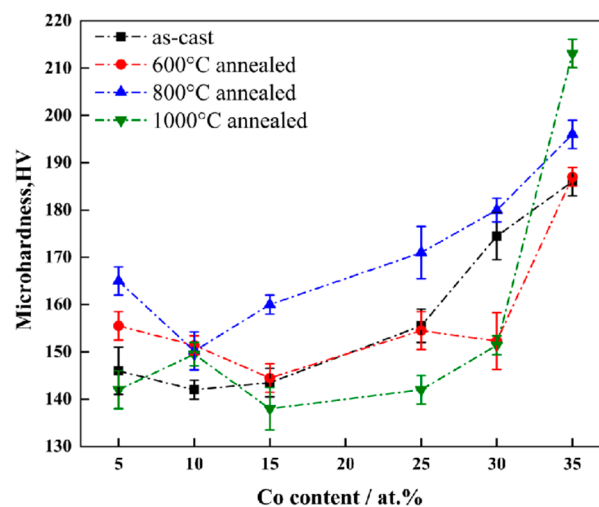


**Figure 6.** Microhardness of the as-cast and annealed  $\text{Co}_x\text{CrFeMnNi}_{2-x}$  alloys.

It is clear that the  $\text{Co}_{35}\text{Ni}_{15}$  alloy annealed at 600 °C has the same microhardness as the as-cast one, and its hardness increased with the annealing temperature. After annealing at 1000 °C, the hardness of the  $\text{Co}_{35}\text{Ni}_{15}$  alloy reaches 213 HV, which is 14% higher than that of the as-cast alloy. It should be noted that the alloys were quenched after annealing and the test was performed at room temperature; thus, a higher annealing temperature leads to more FCC→HCP transformations.

Moreover, as can be seen from Figure 6, the microhardness of the  $\text{Co}_5\text{Ni}_{35}$ – $\text{Co}_{30}\text{Ni}_{10}$  alloys, either in as-cast states or after annealing at 600 or 1000 °C, is around  $145 \pm 6$  HV. After annealing at 800 °C, the microhardness of the  $\text{Co}_{15}\text{Ni}_{25}$  and  $\text{Co}_{25}\text{Ni}_{15}$  alloys increased by 20 HV. This indicates that the BCC precipitate has a limited influence on microhardness [39].

### 3.6. First-Principle Calculations

To understand the phase stability and mechanical properties of the FCC and HCP phases, the total energy and elastic properties of the  $\text{Co}_{35}\text{Cr}_{20}\text{Fe}_{20}\text{Mn}_{20}\text{Ni}_5$  alloy were calculated using the first-principle method. The crystal models were built based on the virtual crystal approximation method (VCA) [29–31]. The ground total energy, phase structure, and mechanical properties were systematically calculated.

The calculated results are presented in Table 2. It is clear that the total energy of the HCP structure is a little lower than that of the FCC structure. That means that the HCP structure is more stable at 0 K. It needs to be pointed out that the difference between the total energy of HCP and FCC crystals is just 0.01 eV/atom; therefore, the  $\text{Co}_{35}\text{Cr}_{20}\text{Fe}_{20}\text{Mn}_{20}\text{Ni}_5$  FCC structure cannot totally transform to HCP structure. The bulk modulus of the HCP structure is a little higher than that of the FCC structure. As for the elastic constant, the

HCP structure has much higher levels of  $C_{11}$  but much lower levels of  $C_{12}$  and  $C_{44}$ . This tendency is the same as that calculated by the results of [40].

**Table 2.** First-principle calculations of  $\text{Co}_{35}\text{Cr}_{20}\text{Fe}_{20}\text{Mn}_{20}\text{Ni}_5$  with FCC and HCP structures.

Structure	Lattice Constant/Å	Elastic Constant/GPa					Total Energy/eV/atom	Bulk Modulus/GPa	Young's Modulus /GPa
		$C_{11}$	$C_{12}$	$C_{13}$	$C_{33}$	$C_{44}$			
FCC	a = 3.4870	298.09	139.91	—	—	150.80	−1166.07	192.63	278.62
HCP	a = 2.4828 c = 3.9783	387.04	130.55	108.95	395.41	89.23	−1166.08	207.33	283.43

#### 4. Discussion

It is well known that the FCC {111} planes and the HCP {0001} planes have the same atom arrangement. The stacking fault of the FCC crystal is equivalent to the formation of a thin HCP structure. Lower SFE (stacking fault energy) can activate deformation twins and stacking faults and promote the FCC to HCP transition. Twin deformation plays an important role in the strengthening and dynamic deformation of low SFE HEAs. The dynamic deformation behavior of FCC HEAs with low SFE is subject to twinning deformation [41,42]. The plastic deformation mechanism should change from dislocation slip to deformation twinning and finally to FCC→HCP transformation. It was reported that no HCP phase was found in the  $\text{Co}_x\text{Cr}_{25}(\text{FeNi})_{75-x}$  alloys with less than 55%Co [18], while the volume fraction of HCP phase reaches 91.3% when Co content reaches 65%. It can also be deduced that the higher Co content, the lower SFE, and the greater degree of FCC to HCP transition.

In the present work, it is found that, when Co content is above 30%, the increase in Co content, at the expense of decreasing Ni content, yields reduced FCC phase stability. The FCC + HCP is stable below 420 °C in the  $\text{Co}_x\text{CrFeMnNi}_{2-x}$  alloys when  $x \geq 1.5$ . The FCC to HCP transition can occur in  $\text{Co}_{1.75}\text{CrFeMnNi}_{0.25}$  alloy during cooling and without strain-inducing, which indicates that the transformation has a large driving force and a fast speed. Moreover, the FCC + HCP is stable below 420 °C, which is different from the strain-induced metastable HCP phase in Ref. [16]. It is a new method to induce an HCP phase and strengthen the FCC high-entropy alloys.

#### 5. Conclusions

1. When  $x \geq 1.5$ , the FCC and HCP phases coexist in the Co-rich  $\text{Co}_x\text{CrFeMnNi}_{2-x}$  alloys at room temperature. They have the same chemical composition, and the volume fraction of the HCP phase increases with Co content.
2. It is confirmed that, in the  $\text{Co}_{1.75}\text{CrFeMnNi}_{0.25}$  alloy, the HCP phase forms during cooling with an FCC→HCP transition around 450 °C. The HCP phase is not stable above 600 °C.
3. As for the  $\text{Co}_{1.75}\text{CrFeMnNi}_{0.25}$  alloy, the HCP structure is more stable than the FCC structure and has a higher bulk modulus.
4. The microhardness of  $\text{Co}_{1.75}\text{CrFeMnNi}_{0.25}$  numero HCP phase reaches 213 HV and is much higher than the other alloys that do not contain an HCP phase, either in their as-cast states or after annealing. The FCC→HCP transformation should improve the alloy's mechanical properties.

**Author Contributions:** Conceptualization, C.W.; Data curation, Y.W., C.W. and M.T.; Formal analysis, Y.W., C.W., Y.L., X.L. and X.S.; Funding acquisition, C.W. and X.S.; Investigation, Y.W. and M.T.; Methodology, C.W.; Project administration, C.W. and Y.L.; Writing—original draft preparation, Y.W.; Writing—review and editing, C.W. and Y.L. All authors have read and agreed to the published version of the manuscript.

**Funding:** This research was funded by financial support from the National Natural Science Foundation of China (Nos. 51771035 and 52271005), the Postgraduate Research & Practice Innovation

Program of Jiangsu Province (No. SJCX21\_1248), and the Priority Academic Program Development of Jiangsu Higher Education Institutions.

**Data Availability Statement:** Not applicable.

**Conflicts of Interest:** The authors declare no conflict of interest.

## References

1. Mishra, R.K.; Kumari, P.; Gupta, A.K.; Shahi, R.R. Design and development of  $\text{Co}_{35}\text{Cr}_5\text{Fe}_{20-x}\text{Ni}_{20+x}\text{Ti}_{20}$  High Entropy Alloy with excellent magnetic softness. *J. Alloys Compd.* **2022**, *889*, 161773. [[CrossRef](#)]
2. Shi, P.; Li, R.; Li, Y.; Wen, Y.; Zhong, Y.; Ren, W.; Shen, Z.; Zheng, T.; Peng, J.; Liang, X.; et al. Hierarchical crack buffering triples ductility in eutectic herringbone high-entropy alloys. *Science* **2021**, *373*, 912–918. [[CrossRef](#)]
3. Bracq, G.; Laurent-Brocq, M.; Perrière, L.; Pirès, R.; Joubert, J.-M.; Guillot, I. The fcc solid solution stability in the Co-Cr-Fe-Mn-Ni multi-component system. *Acta Mater.* **2017**, *128*, 327–336. [[CrossRef](#)]
4. Yeh, J.-W. Alloy Design Strategies and Future Trends in High-Entropy Alloys. *JOM* **2013**, *65*, 1759–1771. [[CrossRef](#)]
5. Tsai, K.Y.; Tsai, M.H.; Yeh, J.W. Sluggish diffusion in Co-Cr-Fe-Mn-Ni high-entropy alloys. *Acta Mater.* **2013**, *61*, 4887–4897. [[CrossRef](#)]
6. Cao, X.; Wu, C.; Liu, Y.; Peng, H.; Su, X. Eutectic Reaction and Microstructure Stability in  $\text{CoCrFeNiNb}_x$  High-Entropy Alloys. *Metals* **2022**, *12*, 756. [[CrossRef](#)]
7. Santodonato, L.J.; Zhang, Y.; Feyngenson, M.; Parish, C.M.; Gao, M.C.; Weber, R.J.; Neufeind, J.C.; Tang, Z.; Liaw, P.K. Deviation from high-entropy configurations in the atomic distributions of a multi-principal-element alloy. *Nat. Commun.* **2015**, *6*, 5964. [[CrossRef](#)]
8. Tian, M.; Wu, C.; Liu, Y.; Peng, H.; Wang, J.; Su, X. Phase stability and microhardness of  $\text{CoCrFeMn}_x\text{Ni}_{2-x}$  high entropy alloys. *J. Alloys Compd.* **2019**, *811*, 152025. [[CrossRef](#)]
9. Pradeep, K.G.; Tasan, C.C.; Yao, M.J.; Deng, Y.; Springer, H.; Raabe, D. Non-equiatomic high entropy alloys: Approach towards rapid alloy screening and property-oriented design. *Mater. Sci. Eng. A* **2015**, *648*, 183–192. [[CrossRef](#)]
10. Youssef, K.M.; Zaddach, A.J.; Niu, C.; Irving, D.L.; Koch, C.C. A Novel Low-Density, High-Hardness, High-entropy Alloy with Close-packed Single-phase Nanocrystalline Structures. *Mater. Res. Lett.* **2015**, *3*, 95–99. [[CrossRef](#)]
11. Senkov, O.N.; Senkova, S.V.; Woodward, C. Effect of aluminum on the microstructure and properties of two refractory high-entropy alloys. *Acta Mater.* **2014**, *68*, 214–228. [[CrossRef](#)]
12. Laurent-Brocq, M.; Perrière, L.; Pirès, R.; Champion, Y. From high entropy alloys to diluted multi-component alloys: Range of existence of a solid-solution. *Mater. Des.* **2016**, *103*, 84–89. [[CrossRef](#)]
13. Cantor, B.; Chang, I.T.H.; Knight, P.; Vincent, A.J.B. Microstructural development in equiatomic multicomponent alloys. *Mater. Sci. Eng. A* **2004**, *375–377*, 213–218. [[CrossRef](#)]
14. Gludovatz, B.; Hohenwarter, A.; Catoor, D.; Chang, E.H.; George, E.P.; Ritchie, R.O. A fracture-resistant high-entropy alloy for cryogenic applications. *Science* **2014**, *345*, 1153–1158. [[CrossRef](#)] [[PubMed](#)]
15. Kawamura, M.; Asakura, M.; Okamoto, N.L.; Kishida, K.; Inui, H.; George, E.P. Plastic deformation of single crystals of the equiatomic Cr-Mn-Fe-Co-Ni high-entropy alloy in tension and compression from 10 K to 1273 K. *Acta Mater.* **2021**, *203*, 116454. [[CrossRef](#)]
16. Wei, D.; Li, X.; Jiang, J.; Heng, W.; Koizumi, Y.; Choi, W.-M.; Lee, B.-J.; Kim, H.S.; Kato, H.; Chiba, A. Novel Co-rich high performance twinning-induced plasticity (TWIP) and transformation-induced plasticity (TRIP) high-entropy alloys. *Scr. Mater.* **2019**, *165*, 39–43. [[CrossRef](#)]
17. Wagner, C.; Ferrari, A.; Schreuer, J.; Couzinié, J.-P.; Ikeda, Y.; Körmann, F.; Eggeler, G.; George, E.P.; Laplanche, G. Effects of Cr/Ni ratio on physical properties of Cr-Mn-Fe-Co-Ni high-entropy alloys. *Acta Mater.* **2022**, *227*, 117693. [[CrossRef](#)]
18. Wei, D.; Li, X.; Heng, W.; Koizumi, Y.; He, F.; Choi, W.-M.; Lee, B.-J.; Kim, H.S.; Kato, H.; Chiba, A. Novel Co-rich high entropy alloys with superior tensile properties. *Mater. Res. Lett.* **2019**, *7*, 82–88. [[CrossRef](#)]
19. Guo, S.; Ng, C.; Lu, J.; Liu, C.T. Effect of valence electron concentration on stability of fcc or bcc phase in high entropy alloys. *J. Appl. Phys.* **2011**, *109*, 103505. [[CrossRef](#)]
20. Fang, W.; Yu, H.; Chang, R.; Zhang, X.; Ji, P.; Liu, B.; Li, J.; Qu, X.; Liu, Y.; Yin, F. Microstructure and mechanical properties of Cr-rich Co-Cr-Fe-Ni high entropy alloys designed by valence electron concentration. *Mater. Chem. Phys.* **2019**, *238*, 121897. [[CrossRef](#)]
21. Chung, D.H.; Kim, W.C.; Baek, S.Y.; Kim, M.H.; Na, Y.S. Thermodynamics-based design strategy for optimizing strength and ductility of Cr-Ni-Mn-Fe medium-entropy alloys. *J. Alloys Compd.* **2022**, *899*, 163331. [[CrossRef](#)]
22. Schuh, B.; Mendez-Martin, F.; Völker, B.; George, E.P.; Clemens, H.; Pippin, R.; Hohenwarter, A. Mechanical properties, microstructure and thermal stability of a nanocrystalline  $\text{CoCrFeMnNi}$  high-entropy alloy after severe plastic deformation. *Acta Mater.* **2015**, *96*, 258–268. [[CrossRef](#)]
23. De Cooman, B.C.; Estrin, Y.; Kim, S.K. Twinning-induced plasticity (TWIP) steels. *Acta Mater.* **2018**, *142*, 283–362. [[CrossRef](#)]
24. Fang, W.; Chang, R.; Ji, P.; Zhang, X.; Liu, B.; Qu, X.; Yin, F. Transformation Induced Plasticity Effects of a Non-Equal Molar Co-Cr-Fe-Ni High Entropy Alloy System. *Metals* **2018**, *8*, 369. [[CrossRef](#)]

25. Wang, Q.; Wu, C.; Xu, X.; Peng, H.; Liu, Y.; Su, X. Effect of Annealing on Microstructure and Corrosion resistance of the  $\text{Co}_x\text{CrFeMnNi}_{2-x}$  High-entropy Alloys. *Mater. Rep.* **2022**, *36*, 21110150.
26. Tian, M.; Wu, C.; Liu, Y.; Peng, H.; Wang, J.; Su, X. Phase stability of the  $\text{Co}_x\text{Mn}_{2-x}\text{CrFeNi}$  high entropy alloys. *Mater. Rep.* **2020**, *34*, 17067–17071.
27. Zhang, F.X.; Zhao, S.; Jin, K.; Bei, H.; Popov, D.; Park, C.; Neuefeind, J.C.; Weber, W.J.; Zhang, Y. Pressure-induced fcc to hcp phase transition in Ni-based high entropy solid solution alloys. *Appl. Phys. Lett.* **2017**, *110*, 011902. [[CrossRef](#)]
28. Gao, X.; Chen, R.; Liu, T.; Fang, H.; Wang, L.; Su, Y. High deformation ability induced by phase transformation through adjusting Cr content in Co-Fe-Ni-Cr high entropy alloys. *J. Alloys Compd.* **2022**, *895*, 162564. [[CrossRef](#)]
29. Tian, F. A Review of Solid-Solution Models of High-Entropy Alloys Based on Ab Initio Calculations. *Front. Mater.* **2017**, *4*, 36. [[CrossRef](#)]
30. Mu, Y.; Liu, H.; Liu, Y.; Zhang, X.; Jiang, Y.; Dong, T. An ab initio and experimental studies of the structure, mechanical parameters and state density on the refractory high-entropy alloy systems. *J. Alloys Compd.* **2017**, *714*, 668–680. [[CrossRef](#)]
31. Bellaiche, L.; Vanderbilt, D. Virtual crystal approximation revisited: Application to dielectric and piezoelectric properties of perovskites. *Phys. Rev. B* **2000**, *61*, 7877–7882. [[CrossRef](#)]
32. King, D.J.M.; Burr, P.A.; Obbard, E.G.; Middleburgh, S.C. DFT study of the hexagonal high-entropy alloy fission product system. *J. Nucl. Mater.* **2017**, *488*, 70–74. [[CrossRef](#)]
33. Gao, Y.; Qiao, L.; Wu, D.; Zhang, Y.; Zou, Y. First principle calculation of the effect of Cr, Ti content on the properties of  $\text{VMoNbTaWM}_x$  ( $M = \text{Cr, Ti}$ ) refractory high entropy alloy. *Vacuum* **2020**, *179*, 109459. [[CrossRef](#)]
34. Tran, N.-D.; Saengdeejing, A.; Suzuki, K.; Miura, H.; Chen, Y. Stability and Thermodynamics Properties of  $\text{CrFeNiCoMn/Pd}$  High Entropy Alloys from First Principles. *J. Phase Equilibria Diffus.* **2021**, *42*, 606–616. [[CrossRef](#)]
35. Liang, F.; Du, J.; Su, G.S.; Xu, C.H.; Zhang, C.Y.; Kong, X.M. Phase stability and mechanical properties analysis of  $\text{AlCo}_x\text{CrFeNi}$  HEAs based on first principles. *Metals* **2022**, *12*, 1860. [[CrossRef](#)]
36. Wu, C.; Zhou, C.; Liu, Y.; Peng, H.; Wang, J.; Su, X. Effects of vacuum annealing on the phase constituents and mechanical properties of the  $\text{Al}_x\text{CrFeMn}_{2-x}\text{Ni}$  multiprincipal component alloys. *Vacuum* **2022**, *199*, 110934. [[CrossRef](#)]
37. Wu, C.; Sun, Y.; Liu, Y.; Tu, H. Effect of Long-Time Annealing at 1000 °C on Phase Constituent and Microhardness of the  $20\text{Co-Cr-Fe-Ni}$  Alloys. *Materials* **2019**, *12*, 1700. [[CrossRef](#)]
38. Chen, H.-L.; Mao, H.; Chen, Q. Database development and Calphad calculations for high entropy alloys: Challenges, strategies, and tips. *Mater. Chem. Phys.* **2018**, *210*, 279–290. [[CrossRef](#)]
39. Edalati, P.; Mohammadi, A.; Tang, Y.; Floriano, R.; Fuji, M.; Edalati, K. Phase transformation and microstructure evolution in ultrahard carbon-doped  $\text{AlTiFeCoNi}$  high-entropy alloy by high-pressure torsion. *Mater. Lett.* **2021**, *302*, 130368. [[CrossRef](#)]
40. Li, X.; Irving, D.L.; Vitos, L. First-principles investigation of the micromechanical properties of fcc-hcp polymorphic high-entropy alloys. *Sci. Rep.* **2018**, *8*, 11196. [[CrossRef](#)]
41. Wang, R.; Tang, Y.; Li, S.; Bai, S. Research progress on deformation mechanisms under dynamic loading of high-entropy alloys. *Mater. Rep.* **2021**, *35*, 17001–17009.
42. Chen, J.; Feng, Z.; Jianhong, Y. Coordination deformation mechanism between dislocation and twin in  $\text{CrCoNi}$  medium entropy alloy. *Mater. Rep.* **2022**, *36*, 20090129.

**Disclaimer/Publisher’s Note:** The statements, opinions and data contained in all publications are solely those of the individual author(s) and contributor(s) and not of MDPI and/or the editor(s). MDPI and/or the editor(s) disclaim responsibility for any injury to people or property resulting from any ideas, methods, instructions or products referred to in the content.